DMD Fast Forward. Published on July 2, 2022 as DOI: 10.1124/dmd.121.000609
This article has not been copyedited and formatted. The final version may differ from this version.

1 Title Page

Title: Physiologically Based Pharmacokinetic Modeling of Vitamin D_3 and Metabolites in Vitamin D Insufficient Patients

Authors: Colton W. Sawyer, Stacey M. Tuey, Raymond E. West III, Thomas D. Nolin, Melanie S. Joy

CWS: Department of Mathematics, Southern New Hampshire University, 2500 N River Rd, Manchester, NH 03106, USA

SMT, MSJ: University of Colorado, Skaggs School of Pharmacy and Pharmaceutical Sciences, 12850 East Montview Blvd, Room 4108, Mail Stop C238 Aurora, CO 80045, USA

REW, TDN: University of Pittsburgh, School of Pharmacy, Department of Pharmacy and Therapeutics, 208 Salk Pavilion, 335 Sutherland Drive, Pittsburgh PA 15261, USA

Corresponding Author: Colton W. Sawyer; (603) 629-3530; fax: (603) 645-9779; email: c.sawyer1@snhu.edu

Laboratories of Data Origin: MSJ and TDN

DMD Fast Forward. Published on July 2, 2022 as DOI: 10.1124/dmd.121.000609
This article has not been copyedited and formatted. The final version may differ from this version.

2 Running Title Page

Running Title: PBPK Model of Vit D_3 and Metabolites

Key Words: Physiologically based pharmacokinetics, mathematical modeling, vitamin D_3, cytochrome P450 (CYP)

Corresponding Author: Colton W. Sawyer; (603) 629-3530; fax: (603) 645-9779; email: c.sawyer1@snhu.edu

Counts:

- Text Pages: 16 main + 3 appendix
- Number of Tables: 2
- Number of Figures: 5 total figures (Figure 3 has three subfigures)
- Number of References: 62
- Number of words in *Abstract*: 213
- Number of words in *Introduction*: 747
- Number of words in *Discussion*: 1498

List of Non-standard Abbreviations:

VitD_3, Vitamin D_3; 25D_3, 25(OH)D_3; 1,25D_3, 1,25$(OH)_2D_3$; 24,25D_3, 24,25$(OH)_2D_3$

DMD Fast Forward. Published on July 2, 2022 as DOI: 10.1124/dmd.121.000609
This article has not been copyedited and formatted. The final version may differ from this version.

3 Abstract

A physiologically based pharmacokinetic (PBPK) model of vitamin D_3 and metabolites [25(OH)D_3, 1,25$(OH)_2D_3$, and 24,25$(OH)_2D_3$] is presented. In this study, patients with 25(OH)D_3 plasma concentrations below 30 ng/ml were studied after a single dose of 5,000 I.U. (125 µg) cholecalciferol, provided with 5,000 I.U. daily cholecalciferol supplementation until vitamin D replete (25(OH)D_3 plasma concentrations above 30 ng/ml), and had serial plasma samples were collected at each phase for 14 days. Total concentrations of vitamin D_3 and metabolites were measured by ultra-high performance liquid chromatography tandem mass spectrometry. A nine-compartment PBPK model was built using MATLAB to represent the triphasic study nature (insufficient, replenishing, sufficient). Stimulatory and inhibitory effect of 1,25$(OH)_2D_3$ were incorporated by fold-changes in the primary metabolic enzymes CYP27B1 and CYP24A1, respectively. Incorporation of dynamic adipose partition coefficients for vitamin D_3 and 25(OH)D_3 and variable enzymatic reactions aided in model fitting. Measures of model predictions agreed well with data from metabolites, with 97%, 88%, and 98% of the data for 25(OH)D_3, 24,25$(OH)_2D_3$, and 1,25$(OH)_2D_3$, respectively, within 2-fold of unity (*fold error* values between 0.5 and 2.0). Bootstrapping was performed and optimized parameters were reported with 95% confidence intervals. This PBPK model could be a useful tool for understanding the connections between vitamin D and its metabolites under a variety of clinical situations.

DMD Fast Forward. Published on July 2, 2022 as DOI: 10.1124/dmd.121.000609
This article has not been copyedited and formatted. The final version may differ from this version.

4 Significance Statement

This study developed a physiologically based pharmacokinetic (PBPK) model of vitamin D_3 and metabolites for patients moving from an insufficient to a repleted state over a period of 16 weeks.

DMD Fast Forward. Published on July 2, 2022 as DOI: 10.1124/dmd.121.000609
This article has not been copyedited and formatted. The final version may differ from this version.

5 Visual Abstract

Not required

DMD Fast Forward. Published on July 2, 2022 as DOI: 10.1124/dmd.121.000609
This article has not been copyedited and formatted. The final version may differ from this version.

6 Introduction

Vitamin D is a fat-soluble, prohormone that plays an essential role in regulating calcium and phosphorus to maintain musculoskeletal health. The main source of vitamin D is through endogenous production of cholecalciferol ($VitD_3$) in the skin upon ultraviolet B exposure from the sun. The active form of $VitD_3$, $1,25(OH)_2D_3$ ($1,25D_3$) has been found to exhibit many pleiotropic actions beyond calcium and phosphorus homeostasis (e.g. musculoskeletal health), that are often referred to as "non-classical" actions. Additionally, $1,25D_3$ controls over 200 genes, including those responsible for the regulation of hormone secretion, immune function, and cell proliferation and differentiation [Holick, 2006].

VitD insufficiency is a global health issue and it has been estimated that up to 80% of men and women in the United States of America (USA), Canada, and Europe meet this classification [Ganji et al., 2012; van Schoor and Lips, 2018]. VitD status is based on concentrations of 25-hydroxyvitamin D, 25(OH)D (25D), given that it is the major circulating form and it is readily assayed in hospital laboratories. There is a lack of consensus on the serum concentrations of 25D considered to be adequate, but it is commonly agreed that 25D concentrations should be above 20 ng/ml (1 ng/ml = 2.5 nmol/l) [Ganji et al., 2012, van Schoor and Lips, 2018]. The Institute of Medicine (IOM) defines deficiency as 25D < 12 ng/ml and recommends a target serum concentration of 20 ng/ml [Ross, 2011]. The Endocrine Society (ENDO) defines VitD deficiency as 25D < 20 ng/ml and recommends a target concentration of 30 ng/ml [Holick et al., 2011]. However, other leading experts define VitD insufficiency as 25D concentrations between 20 and 30 ng/ml and deficiency as concentrations < 20 ng/ml [Cianferotti and Marcocci, 2012; Dawson-Hughes et al., 2005; Holick, 2007; Holick et al., 2011]. While many people with VitD insufficiency take supplements, treatment recommendations are not consistent. The IOM recommended a daily intake of 600 I.U. VitD for children, adolescents, and adults, and 800 I.U. for adults over the age of 70 to maintain 25D concentrations of 20 ng/ml [Jernigan and Andress, 2003]. ENDO recommended 1500-2000 I.U./day to prevent or treat VitD insufficiency and achieve 25D concentrations above 30 ng/ml, with a preferred range of 40-60 ng/ml [Holick et al., 2011]. While these are the common guidelines in the U.S., recommendations in other

DMD Fast Forward. Published on July 2, 2022 as DOI: 10.1124/dmd.121.000609
This article has not been copyedited and formatted. The final version may differ from this version.

regions of the world differ based on many population-specific factors such as sunlight exposure, skin pigmentation, clothing, and dietary practices [Haq et al., 2018; Munns et al., 2016; Pérez-López et al., 2012; Płudowski et al., 2013; Rizzoli et al., 2013; Society, 2012].

Activation of VitD occurs through two sequential hydroxylation steps to generate the metabolically active metabolite 1,25D. Vitamin D is hydroxylated in the liver primarily by the cytochrome P450 (CYP) enzyme CYP2R1, but also through pathways with CYP27A1 [Sakaki et al., 2005] and CYP3A4 [Battault et al., 2012; Wang et al., 2013], to form 25D, the major circulating metabolite. 25D can then be hydroxylated in the kidney by either CYP27B1 to the active metabolite, 1,25D, or by CYP24A1 to the inactive metabolite 24,25-dihydroxyvitamin D (24,25D). Phase 2 metabolism pathways have also been described for VitD but appear to be of lesser importance [Gao et al., 2017; Wang et al., 2014; Wong et al., 2018]. 1,25D is tightly regulated in a feedback loop with CYP27B1 and CYP24A1; high concentrations of 1,25D will respectively suppress and stimulate expressions of CYP27B1 and CYP24A1.

Despite VitD being used clinically for decades, there are a limited number of published studies that include assessments of the parent VitD compound and metabolites using pharmacokinetic or physiologically based pharmacokinetic (PBPK) approaches [Armas et al., 2004; Bailie and Johnson, 2002; Benaboud et al., 2013; Fassio et al., 2020; Hsu et al., 2021; Ilahi et al., 2008; Jetter et al., 2014; Kimura et al., 1991; Levine and Song, 1996; Meekins et al., 2014;, Ocampo-Pelland et al., 2016, 2017; Ramakrishnan et al., 2016; Roth et al., 2012]. The current study sought to develop a PBPK model of $VitD_3$ and metabolites in VitD insufficient patients in the U.S. who were treated with moderate (5000 I.U.) daily doses of $VitD_3$ for up to 16 weeks to achieve replacement as defined by 25D $\geq$ 30 ng/ml. Through establishing a model that might align well with a triphasic clinical experience of a patient–an initial visit for establishing VitD concentrations, time to achieve repletion on a dosing regimen, and a follow-up visit–this study aimed to better understand the longitudinal effects of daily supplementation of moderate doses of $VitD_3$.

DMD Fast Forward. Published on July 2, 2022 as DOI: 10.1124/dmd.121.000609
This article has not been copyedited and formatted. The final version may differ from this version.

7 Materials and Methods

7.1 Design Overview

The parent study from which the data was obtained was carried out in accordance with the Declaration of Helsinki. All subjects provided informed consent and the protocols were approved by the Institutional Review Boards at the University of Colorado and the University of Pittsburgh. The parent study (NCT02360644) was registered under ClinicalTrials.gov and can be referenced for additional details.

7.1.1 Study Participants

Healthy subjects from the University of Colorado and University of Pittsburgh with VitD insufficiency defined in the study as total 25D below 30 ng/ml and not receiving VitD replacement therapy were recruited. Other eligibility criteria included age 18-75 years, predicted compliance with study visits, not pregnant or lactating, no changes in medications within 4 weeks, no predisposition to hypercalcemia, and hemoglobin ≥ 10 g/dL. Exclusion criteria were active autoimmune disease, active or recent infections requiring antimicrobial treatment and hepatic insufficiency. Note that while the parent clinical study focused on patients with chronic kidney disease, this study utilized data from a control group of healthy study participants from the parent clinical study. Baseline characteristics for study participants (n=11) can be found in Table 1.

7.1.2 Clinical Study Design

Vitamin D insufficient subjects were admitted to the Clinical and Translational Research Centers (CTRC) at the University of Colorado or University of Pittsburgh for a 12 h stay, followed by visits at 24, 48, 168, and 336 h. Participants were required to be fasting at the beginning of the study. Any prescribed medications were withheld for the first two hours of the study. Subjects were given a single 5,000 I.U. (125 μg) oral dose of $VitD_3$ (Jarrow Formulas, Los Angeles, CA). Serial blood samples (7.5 ml) were collected at baseline and at 0.5, 1, 2, 4, 8, 12, 24, 48, 168, and 336 h into heparinized vacutainers. Blood samples were centrifuged immediately following collection for 10 min at 3000 xG at 4◦C and plasma samples were stored at -80◦C until analysis. After the 336 h

DMD Fast Forward. Published on July 2, 2022 as DOI: 10.1124/dmd.121.000609
This article has not been copyedited and formatted. The final version may differ from this version.

blood draw, participants were given up to 16 weeks of daily supplementation of 5000 I.U. $VitD_3$ to attain replete concentrations (≥ 30 ng/ml). At the repleted study phase, participants were given a final dose of 5,000 I.U. $VitD_3$ followed by collection of blood samples as previously described for up to 336 h. The total study reflected three phases–the insufficient phase, the replenishing phase, and the repleted phase. Data are available for subjects in the insufficient and repleted phases.

7.1.3 Analytical Assay

Total concentrations of $VitD_3$ and metabolites [$25D_3$, $1,25D_3$, and $24,25D_3$] were determined by a novel ultra-high performance liquid chromatography-tandem mass spectrometry (UHPLC-MS/MS) assay capable of detecting all four analytes simultaneously as previously described [Stubbs et al., 2014] with minor modifications. UHPLC was performed with a Waters Acquity UPLC I-class (Waters, Milford, MA, USA), which includes a sample manager and a binary solvent manager. Briefly, 500 µl samples were precipitated with acetonitrile, extracted with methyl tert butyl ether, then derivatized with 4-phenyl-1,2,4-triazoline-3,5dione. Separation of derivatized VitD analytes was achieved using a Waters Acquity BEH C18 column (150 mm × 2.1 mm, 1.7 µm particles) with a gradient elution of water with 0.1% formic acid and acetonitrile. The flow rate was 500 µl/min and the total run time was 8 min. Detection of analytes was achieved using positive atmospheric pressure chemical ionization and selected reaction monitoring on a TSQ Quantum Ultra triple quadrupole mass spectrometer (Thermo Scientific, San Jose, CA). Standards and quality control samples were constructed using blank human serum. Standard curve ranges were 0.10-15 ng/ml for $VitD_3$ and $24,25D_3$, 0.0100-0.500 ng/ml for $1,25D_3$, and 1.0-100 ng/ml for $25D_3$. Mean correlation coefficients were ≥ 0.994 for all calibration curves. The within-run and between-run accuracy and precision percentage coefficient of variation were < 10.6% for all analytes.

7.2 Physiologically Based Pharmacokinetic Model Development

A nine-compartment PBPK model (adipose tissue, brain, heart, kidney, liver, rapidly perfused tissue, slowly perfused tissue, and plasma) was developed for $VitD_3$ and its metabolites using MATLAB (version R2020a, The

DMD Fast Forward. Published on July 2, 2022 as DOI: 10.1124/dmd.121.000609
This article has not been copyedited and formatted. The final version may differ from this version.

Mathworks Inc, Natick, MA). A schematic of the overall PBPK model for each compound is shown in Figure 1 with the connections between each metabolite PBPK model shown in Figure 2.

Physiological parameters were obtained from a previous publication [Davies and Morris, 1993]. The slowly perfused compartment was composed of skin and muscle. The rapidly perfused compartment served as a mass balance compartment and comprised all tissue not previously named. Fractional blood flow rate for the slowly perfused compartment was equal to the sum of the rates of its components. The fractional blood flow rate of the rapidly perfused compartment was equal to the remaining fractional blood flow rates. Following the methods of Ramakrishnan et al. [2016], this study assumed no binding to red blood cells and scaled the blood flow to tissues by multiplying the blood flow Q_B and the blood volume V_B by BP, the blood:plasma ratio, to model the rate of flow of plasma, as shown in Equations (1) and (2):

$$V_P = BP \cdot V_B \quad (1)$$

$$Q_P = BP \cdot Q_B \quad (2)$$

The PBPK model was comprised of conventional mass balance equations assuming well-stirred distribution into each model compartment, with detailed equations for the PBPK model found in the Appendix (Equations (A1) to (A14)). Calculations for relevant partition coefficients and physiological values used in this study are found in the supplemental materials (Supp. Table S1 and S2).

7.2.1 Metabolic Routes

The metabolic cascade for $VitD_3$ considered in this study consists of three CYP enzymes: CYP2R1, CYP27B1, and CYP24A1. Although the CYP enzyme CYP2R1, a microsomal enzyme found mainly in the liver, is primarily responsible for the 25-hydroxylation of $VitD_3$ to $25D_3$ following Michaelis-Menten kinetics [Cheng et al., 2004; Shinkyo et al., 2004], there are several other enzymatic pathways that may be involved in the 25-hydroxylation pathway including CYP27A1 [Sakaki et al., 2005], CYP2J2 and CYP3A4 [Battault et al., 2012; Wang et al.,

DMD Fast Forward. Published on July 2, 2022 as DOI: 10.1124/dmd.121.000609
This article has not been copyedited and formatted. The final version may differ from this version.

2013]. This study chose to focus on the actions of CYP2R1, with the assumption that V_{max} may vary depending on levels of sufficiency [Abramson, 1986]. The variable rate of V_{max} is given by Equation (3):

$$V_{max} = \frac{V'}{1 + \left(\frac{[D]}{D_{50}}\right)^{h_V}}, \quad (3)$$

where V' is the maximum value of V_{max}, $[D]$ is the total liver concentration of $VitD_3$, D_{50} is the concentration at which 50% of the inhibition occurs, and h_V is the Hill coefficient for this function. The conversion of $VitD_3$ to $25D_3$ by CYP2R1 is given by standard Michalis-Menten kinetics (Equation (4)) [Ocampo-Pelland et al., 2016]:

$$CL_D = \frac{V_{max} * [D]}{K_m + [D]}. \quad (4)$$

Endogenous production of $VitD_3$ through incidental exposure to sunlight and additional dietary sources are incorporated into the model using Equation (4). This follows the assumption that the input rate for $VitD_3$ is equal to the output rate of $VitD_3$ to $25D_3$ when there is no external supplementation at low baseline concentrations of $VitD_3$ [Ocampo-Pelland et al., 2016]. Following the approach of Ramakrishnan et al. [2016], the baseline concentration of $VitD_3$ and its metabolites in tissue were calculated using the relationship between measured total plasma concentrations and partition coefficients as $C_{T,base} = P_{T:p} \cdot C_{plasma,base}$, where $C_{T,base}$ is the baseline concentration in tissue T, $P_{T:p}$ is the calculated tissue:plasma partition coefficient, and $C_{plasma,base}$ is the baseline concentration of the compound in the plasma compartment.

The metabolite $25D_3$ is further converted to either $1,25D_3$ by the 1α-hydroxylase CYP27B1, or deactivated to the metabolite $24,25D_3$ by the 24-hydroxylase CYP24A1. Both CYP27B1 and CYP24A1 are renal mitochondrial enzymes which have the capability to demonstrate Michaelis-Menten kinetics [Inouye and Sakaki, 2001; Sakaki et al., 2005]. However, since observed concentrations of $25D_3$ range roughly 20-50 times smaller than literature values of K_m for CYP27B1 [Inouye and Sakaki, 2001] and 200-400 times smaller than literature values of K_m for CYP24A1 [Sakaki et al., 2005], this study assumes linear first-order kinetics for CYP27B1 and CYP24A1 acting on $25D_3$.

DMD Fast Forward. Published on July 2, 2022 as DOI: 10.1124/dmd.121.000609
This article has not been copyedited and formatted. The final version may differ from this version.

Supplementation doses of $VitD_3$ during the replenishment period were incorporated into the model through pulsing the initial condition for A_{gut}, the amount of oral $VitD_3$ effectively introduced in the intestine en route to the liver. During the initial and final portions of the study where no daily supplements were given, the only source of input to the model is through the endogenous production of $VitD_3$ throughout sunlight and diet. For the purposes of continuity of the model, all participants were assumed to have 16 weeks of supplementation to achieve sufficient concentrations of $25D_3$.

7.2.2 Dynamic Adipose Partition Coefficients

Previous publications have suggested the possibility that partition coefficients in tissues, in particular the kidney, may change with levels of sufficiency [Quach et al., 2015] and the adipose tissue [Sawyer et al., 2017]. We chose to incorporate dynamic partitioning for the adipose tissue compartment for $VitD_3$ and $25D_3$ similar to [Sawyer et al., 2017] using the following equations (Equations (5) and (6)):

$$AdiPC_D(t) = \frac{Adi_{D,max}}{1 + \left(\frac{Adi_{D,50}}{[D]}\right)^{h_D}} \quad (5)$$

$$AdiPC_{25D}(t) = \frac{Adi_{25,max}}{1 + \left(\frac{[25D]}{Adi_{25D,50}}\right)^{h_{25}}} \quad (6)$$

Here, $AdiPC_{[]}(t)$ are the adipose partition coefficients at any point in t related directly to the total plasma concentration of either $VitD_3$ or $25D_3$ at time t (indicated by $[D]$ and $[25D]$, respectively), $Adi_{[],50}$ is the concentration of $VitD_3$ or $25D_3$ at which 50% of the inhibition occurs, and $h_{[]}$ is the Hill coefficient for these functions.

7.3 Stimulatory and inhibitory effects of $1,25D_3$

Circulating and tissue concentrations of $1,25D_3$ are tightly regulated through its synthesis by CYP27B1 and degradation by CYP24A1. CYP27B1 expression is tightly regulated by parathyroid hormone and $1,25D_3$, where

DMD Fast Forward. Published on July 2, 2022 as DOI: 10.1124/dmd.121.000609
This article has not been copyedited and formatted. The final version may differ from this version.

high levels of $1,25D_3$ suppress expression of CYP27B1 [Schuster, 2011]. Conversely, the expression of CYP24A1 is enhanced by the presence of $1,25D_3$; upregulation of CYP24A1 by $1,25D_3$ serves as feedback control to reduce concentrations of $1,25D_3$ [Ramakrishnan et al., 2016]. To incorporate the regulatory effects of $1,25D_3$ plasma concentrations, this study follows the approach previously outlined [Ramakrishnan et al., 2016] and adjusts the fold change (FC; ratio of changed/basal mRNA levels) of CYP27B1 and CYP24A1 in proportion to total $1,25D_3$ plasma concentrations calculated from the partition coefficient in the relevant tissues. The rate of CYP27B1 fold change was expressed as shown in Equation (7):

$$\frac{dCYP27B1_{FC}}{dt} = k_{in,27} \cdot \left(1 - \frac{I_{\max}\,[1,25\mathrm{D_K}]^{\gamma_2}}{IC_{50}^{\gamma_2} + [1,25D_K]^{\gamma_2}}\right) - k_{out,27} \cdot CYP27B1_{FC} \quad (7)$$

with I_{max} the maximum inhibitory effect, IC_{50} the total plasma concentration of $1,25D_3$ in the kidney to achieve 50% of I_{max}, γ_2 is the Hill coefficient for CYP27B1 in the kidney, and $[1,25D_K]$ is the total concentration of $1,25D_3$ in the kidney [Ramakrishnan et al., 2016]. For CYP24A1, Equation (8) gives the fold change in tissue T, for T liver, kidney, intestine, or brain:

$$\frac{dCYP24A1_{FC,T}}{dt} = k_{in,24,T}\left(1 + \frac{E_{\max,\mathrm{T}}\,[1,25\mathrm{D}_T]^{\gamma_{1,T}}}{EC_{50,T}^{\gamma_1} + [1,25D_T]^{\gamma_{1,T}}}\right) - k_{out,24,T} \cdot CYP24A1_{FC,T} \quad (8)$$

where $E_{max,T}$ is the maximum stimulatory effect in tissue T, $EC_{50,T}$ is the total plasma concentration of $1,25D_3$ in the tissue to achieve 50% of E_{max}, $\gamma_{1,T}$ is the Hill coefficient for CYP24A1 in the tissue, and $[1,25D_T]$ is the total concentration of $1,25D_3$ in the tissue [Ramakrishnan et al., 2016]. Following the methods of [Noh et al., 2020, Ramakrishnan et al., 2016], $k_{in,[]}$ and $k_{out,[]}$ are presumed to have the same value but different (appropriate) units for the differential equation.

7.4 Model simulations and parameter estimations

This study follows the approach outlined by McNally et al. [2011] to explore the global sensitivity of the kinetic parameters for this PBPK model. The model equations were coded in MATLAB (version R2020a, The Mathworks Inc, Natick, MA) and sensitivity analysis was conducted using the SAFE Toolbox [Pianosi et al.,

DMD Fast Forward. Published on July 2, 2022 as DOI: 10.1124/dmd.121.000609
This article has not been copyedited and formatted. The final version may differ from this version.

2015]. For the initial analysis, Morris' Method was used to distinguish between the set of influential and noninfluential parameters through ranking [Morris, 1991]. Parameters in this study were considered influential if the normalized mean sensitivity measure obtained using Morris' Method was greater than 0.1 [Hsieh et al., 2018]. Using this method, the set of influential parameters were chosen for optimization and all other parameters were held at available literature values. If a parameter did not have an available literature value, it was also included in the set chosen for optimization.

This set of parameters was optimized using nonlinear least squares where the cost of fit was calculated using the least squares difference between the observed and predicted model data. To avoid unfairly skewing the model, each compound's data were transformed by subtracting the minimum observed value and dividing by the interquartile range of the observed data for that compound. Data were further weighted by the count of the number of available points for optimization in each phase; this ensured that data below the analytical level of quantification were not considered in and did not negatively affect the optimization routine. This was present primarily in the insufficient $VitD_3$ data and comprised approximately 15% of the overall data points (3% of points without the insufficient $VitD_3$ data) used for optimization. The lack of data due to patient $VitD_3$ concentrations below the limit of quantification poses some issue for initialization of the model for this compartment; however, the set of influential parameters span the entire timespan of the model, so we used visual inspection of the curve of the model prediction to assess fit in this area for this compartment. The model was initialized to the mean of the first two time points ($t = 0$ and $t = 0.5$ hours).

To generate 95% confidence intervals for the optimized parameters, a bootstrapping method was used after initial optimization of the model. For this method, parameters identified as candidates for optimization were allowed to vary two-fold from their optimized values, which were based on available literature values, or the best result from multiple iterative guesses. Bootstrapping was performed by systematically running the optimization solver over randomly sampled parameters within these constraints, holding non-optimized parameters constant at literature values. The resulting parameter output range for each optimized parameter was then subject to standard

DMD Fast Forward. Published on July 2, 2022 as DOI: 10.1124/dmd.121.000609
This article has not been copyedited and formatted. The final version may differ from this version.

bootstrapping techniques and the 95% confidence intervals were found for each parameter. To generate a 95% confidence interval around the optimized model, parameters were randomly sampled in a normal distribution from a two-fold range of their optimized value for 50 samples, the model run over these parameter sets, and then the 95th percentile of the total model outputs at every half-hour mark was used to generate the total band for the duration of the time-course data.

7.5 Assessment of Prediction Accuracy

The accuracy of the PBPK predictions was evaluated on predicted plasma concentration fit to observations for the three measured compounds. The predicted plasma concentration was formulated using the set of optimized parameters developed from the bootstrapping results. The goodness of prediction for each compound was based on the average fold error (*AFE*), root mean square error (*RMSE*), and the normalized root mean square error (*NRMSE*) [Sheiner and Beal, 1981]. The *fold error* [Equation (9)], *AFE* [Equation (10)], *RMSE*, [Equation (11)], and *NRMSE* [Equation (12)] were calculated as follows:

$$fold\ error = \frac{Predicted}{Observed} \tag{9}$$

$$AFE = exp\left(\frac{\sum ln(fold\ error)}{n}\right) \tag{10}$$

$$RMSE = \sqrt{\frac{\sum(Pred - Obs)^2}{n}} \tag{11}$$

$$NRMSE = \frac{RMSE}{IQR(\mathrm{Obs})} \tag{12}$$

where *Pred* is the predicted value, *Obs* is the observed value, IQR(*Obs*) is the interquartile range of the observed values, and *n* is the number of observed samples.

DMD Fast Forward. Published on July 2, 2022 as DOI: 10.1124/dmd.121.000609
This article has not been copyedited and formatted. The final version may differ from this version.

8 Results

A basic PBPK approach was applied to $VitD_3$ and metabolites using intrinsic clearance parameters determined from the published literature and physiological distribution parameters (Figure 1). Data from eleven subjects (demographics given in Table 1) were used to fit the model; two subjects withdrew from the study before the conclusion of the experiment.

Due to limited $VitD_3$ time course data, the nearly instantaneous conversion of $VitD_3$ to $25D_3$ in VitD deficient individuals [Heaney et al., 2008], and the adipose tissue as a storage compartment that may contribute to circulating levels of $VitD_3$ [Best et al., 2020], our model was insufficient at predicting available $VitD_3$ time course data (results not shown). However, clinically, $VitD_3$ levels are not measured and not likely to be important since therapy decisions are based on $25D_3$ levels. All optimized and literature model parameters are reported in Table 2. Bootstrapping was performed and optimized parameters are reported with 95% confidence intervals.

The observed and final model predicted concentrations for $25D_3$, $24,25D_3$ and $1,25D_3$ during the insufficient and repleted periods are shown in Figure 3 (a-c), respectively, with a 95% confidence interval band around the optimized parameter model as described in section 7.5. Detailed model predictions for the insufficient and repleted periods are shown as insets in Figure 3. The wavy line in the center of the plots indicate a break in the supplementation period for better clarity on the insufficient and repleted period.

Predictive performance of the PBPK model for the insufficient and repleted periods are shown in Figure 4. The average fold error (*AFE*) for the $VitD_3$ metabolites ranges between 1.01 and 1.05 and the normalized root mean square error (*NRMSE*) ranges between 0.26 and 0.38. *AFE* values close to one and *NRMSE* close to zero are indicative of better model fits to data. The correlation of determination (R^2) for each metabolite is 0.77, 0.67, and 0.63, respectively, and 0.92 when considering all data points together. When considering the *fold error* values for the data, the model performed well with 97%, 88%, and 98% of the data for $25D_3$, $24,25D_3$, and $1,25D_3$,

DMD Fast Forward. Published on July 2, 2022 as DOI: 10.1124/dmd.121.000609
This article has not been copyedited and formatted. The final version may differ from this version.

respectively, within 2-fold of unity (*fold error* values between 0.5 and 2.0). When considering a tighter range of fold error (1.5-fold of unity, with *fold error* values between 0.67 and 1.5), the model performs adequately with nearly 80% of $25D_3$ and $1,25D_3$ captured within a 1.5-*fold error* of unity. $24,25D_3$ data was captured less well, with a 1.5-*fold error* value of 63%.

DMD Fast Forward. Published on July 2, 2022 as DOI: 10.1124/dmd.121.000609
This article has not been copyedited and formatted. The final version may differ from this version.

9 Discussion

Vitamin D insufficiency is highly prevalent in the community, afflicting up to 80% of men and women in the USA, Canada, and Europe [Ganji et al., 2012; van Schoor and Lips, 2018]. While the definitions of VitD insufficiency (and deficiency) are not standardized across medical organizations, targeted concentrations are generally in the 20 ng/ml to 40 ng/ml range for 25D, the primary metabolite used for classification [Ganji et al., 2012; Holick et al., 2011; Ross et al., 2011; van Schoor and Lips, 2018]. While various treatment recommendations have also been proposed according to the IOM [Jernigan and Andress, 2003] and ENDO [Holick et al., 2011], there is variability in success of achieving target concentrations of $25D_3$ in patients. There is currently not a clinically established approach to enable prediction of plasma 25D concentrations that might result from a given treatment regimen for a given patient. There is further complication since the plasma concentration of 25D will be impacted by the function of numerous CYP enzymes through activation and deactivation pathways, as well as through sunlight exposure, skin pigment, diet, and clothing. PBPK modeling has a potential to predict expected plasma concentrations of 25D and subsequent metabolites after administration of oral VitD therapy. The current study reports the development of a PBPK model of $VitD_3$ and metabolites in VitD insufficient subjects in the U.S. who were treated with moderate doses (5,000 I.U.) of daily $VitD_3$ for up to 16 weeks to achieve replacement as defined by 25D ≥ 30 ng/ml. The comprehensive PBPK model for $VitD_3$ incorporated dynamic adipose:plasma partition coefficients, atypical kinetics for CYP2R1 using a variable V_{max} based on the total liver concentration of $VitD_3$, and inhibitory and stimulatory effects of $1,25D_3$ for CYP27B1 and CYP24A1. The resultant model sufficiently predicted the concentrations of $VitD_3$ metabolites well in healthy subjects throughout a multiphase study that incorporated an insufficient phase and replete phase. The model informs an understanding of the disposition of $VitD_3$ metabolites and could be utilized to predict plasma concentrations that might result from a given dosing regimen of $VitD_3$ in human patients.

The developed PBPK model for $VitD_3$ and its metabolites consisted of nine compartments (adipose tissue, brain, heart, intestines, kidney, liver, rapidly perfused tissue, slowly perfused tissue, and plasma). Partition coefficients

DMD Fast Forward. Published on July 2, 2022 as DOI: 10.1124/dmd.121.000609
This article has not been copyedited and formatted. The final version may differ from this version.

were either selected from the literature or calculated as described in the Supplemental Material. Although a previous publication in mice suggested that partition coefficients may differ in states of vitamin D deficiency [Quach et al. 2015], our simulations showed less than a 2% change in liver partition coefficients (as defined by the ratio of liver concentration to plasma concentration) between insufficient and sufficient states for $VitD_3$ and metabolites, and less than 1% for kidney partition coefficients (data not shown). However, we did find a difference in model outcomes with the inclusion of variable partitioning in the adipose tissue compartment. As subjects in our study were initially at levels of insufficiency, there is evidence to suggest that normal daily inputs and endogenous production of vitamin D is not sufficient for accumulation in tissues [Heaney et al., 2009]; however, at higher levels of sufficiency, the body is able to store $VitD_3$ and $25D_3$ in adipose tissue for use at a later time [Abbas, 2017; Heaney et al., 2009; Mawer et al., 1972]. The addition of a variable adipose partition coefficient for VitD and 25D, as described in section 7.2.2 and discussed in [Sawyer et al., 2017] led to enhanced fits for the model. In addition, our model agrees well with previously published human studies without Kp values defined [Holick et al., 2008, figure 2B].

As $VitD_3$ is acquired endogenously through the skin from the effects of ultraviolet-B light on 7-dehydrocholesterol (7-DHC) and dietary sources including dairy and fish, these contribute to baseline concentrations of $VitD_3$ in the plasma. The PBPK model incorporated endogenous $VitD_3$ levels with an assumption of output to $25D_3$. After oral ingestion and absorption of supplemental $VitD_3$, the free fraction is taken up in the liver where it is hydroxylated by 25-hydroxylase to form calcifediol or $25D_3$. Subsequently, $25D_3$ is hydroxylated by the kidneys to form calcitriol or $1,25D_3$, which is considered the most active metabolite of $VitD_3$. The current PBPK model used linear first order kinetics for CYP27B1 and CYP24A1 based on the significantly lower $25D_3$ concentrations vs. published K_m values for the respective enzymes. Supplemental dosing of cholecalciferol was incorporated into the model through pulsing the amount introduced into the intestines.

Circulating and tissue concentrations of $1,25D_3$ are tightly regulated through the synthesis by CYP27B1 and degradation by CYP24A1. While CYP27B1 expression is tightly regulated by the binding of $1,25D_3$ and

DMD Fast Forward. Published on July 2, 2022 as DOI: 10.1124/dmd.121.000609
This article has not been copyedited and formatted. The final version may differ from this version.

parathyroid hormone [Schuster, 2011], the expression of CYP24A1 is enhanced by the presence of $1,25D_3$; upregulation of CYP24A1 by $1,25D_3$ serves as a feedback control to reduce concentrations of $1,25D_3$ [Ramakrishnan et al., 2016]. The current PBPK model incorporated the regulatory effects of $1,25D_3$ plasma concentrations by adjusting the fold change of CYP27B1 and CYP24A1 in proportion to $1,25D_3$ plasma concentrations in the liver, kidney, intestine, and brain, as previously identified [Ramakrishnan et al., 2016]. While the fold-change data was simulated and although the dosing regimen and the supplementation in [Ramakrishnan et al., 2016] is different than our dosing regimen and supplementation, we observed the same general behavior for the fold change of each enzyme (results not shown), namely that as the level of $1,25D_3$ increases, the fold change of CYP27B1 decreases and the levels of CYP24A1 increase in each compartment. When the supplementation was removed at the repleted portion of the study, we observed an expected increase and decrease, respectively, in the fold changes of the CYP24A1 and CYP27B1 enzymes comparative to the concentration of $1,25D_3$ in the appropriate compartments. This behavior follows the expected directions for CYP27B1 and CYP24A1 given the critical concentration of $1,25D_3$ governing these physiological effects on these enzymes.

Recent publications have discussed the advancement of atypical Michaelis-Menten kinetics for a variety of CYP enzymes, including several enzymes involved in the secondary metabolism cascade for vitamin D. This includes CYP3A4 [Arendse et al, 2013] and CYP2J2 [Leow and Chan, 2019; Leow et al., 2021]. In particular, CYP2J2 shares 72.5% sequence similarity with CYP2R1, so it is not unreasonable to assume that CYP2R1 may also exhibit atypical Michaelis-Menten kinetics at varying sufficiency levels. To model this, we chose to use a modification on substrate inhibition kinetics, as shown in Equation (3). This led to strong improvement of model predictions, particularly in latter time points (data not shown).

Since the metabolites versus the parent $VitD_3$ compound are measured clinically to assist clinicians in determining whether patients are $VitD_3$ insufficient and/or whether they require changes to dosing regimens, we performed some simulations of predicted concentrations with common regimens. A simulation using the current model was

DMD Fast Forward. Published on July 2, 2022 as DOI: 10.1124/dmd.121.000609
This article has not been copyedited and formatted. The final version may differ from this version.

performed inputting a dose of 1000 I.U./daily, which is consistent with dosing recommendation according to the IOM. Our model predicted $25D_3$ plasma concentrations well (Figure 5) and is consistent with a previous study with this dosing regimen [Holick et al., 2008, fig. 2B]. Note subjects in [Holick et al., 2008] began the study with sufficient levels of VitD; we hypothesis this explains the slight underprediction of our model to participant data at later time points as the ratio of $VitD_3$ and metabolites may not remain the same across levels of sufficiency for initialization of the model.

Overall, the developed PBPK model of $VitD_3$ that incorporated data from insufficient participants into a repleted phase after daily administration of 5000 I.U. $VitD_3$ for 12-16 weeks led to acceptable and satisfactory predictions in healthy human subjects. When considering the *fold error* values for the data, the model performed well with 97%, 88%, and 98% of the data for $25D_3$, $24,25D_3$, and $1,25D_3$, respectively, within 2-fold of unity (*fold error* values between 0.5 and 2.0). Due to limited $VitD_3$ time course data, the nearly instantaneous conversion of $VitD_3$ to $25D_3$ in VitD deficient individuals [Heaney et al., 2008], and the adipose tissue as a storage compartment that may contribute to circulating levels of $VitD_3$ [Best et al., 2020], our model was insufficient at predicting available $VitD_3$ time course data (results not shown). However, this may not be overly relevant since $VitD_3$ levels are not measured or used clinically. An additional limitation to this model is the lack of available experiemental data for comparison of atypical kinetic parameters for CYP2R1; however, the inclusion of the atypical kinetics greatly improved our model behavior and is within the realm of biological possibility. The model serves to inform an understanding of $VitD_3$ and metabolite disposition and could be utilized to predict $25D_3$ plasma concentrations that might result from a given dosing regimen in human patients. A beneficial future addition to this study would include incorporation of patient-specific data throughout the supplementation phase to better inform the model predictions. This model has applications in studying the effects of repletion schemes for populations of patients with impaired enzymatic abilities, such as chronic kidney disease, an important diseased population we are currently evaluating.

DMD Fast Forward. Published on July 2, 2022 as DOI: 10.1124/dmd.121.000609
This article has not been copyedited and formatted. The final version may differ from this version.

10 Acknowledgements

We wish to thank University of Colorado and the University of Pittsburgh for their help in the conduct of the clinical studies. Jarrow Formulas, Inc. (Los Angeles, CA) is gratefully acknowledged for providing study drug (cholecalciferol 5,000 I.U.).

DMD Fast Forward. Published on July 2, 2022 as DOI: 10.1124/dmd.121.000609
This article has not been copyedited and formatted. The final version may differ from this version.

11 Authorship Contributions

Participated in research design: Joy and Nolin

Conducted experiments: Joy, Nolin, Tuey, and West

Performed data analysis: Sawyer

Wrote or contributed to the writing of the manuscript: Sawyer, Tuey, Joy, and Nolin

DMD Fast Forward. Published on July 2, 2022 as DOI: 10.1124/dmd.121.000609
This article has not been copyedited and formatted. The final version may differ from this version.

12 References

Abbas MA (2017) Physiological functions of vitamin D in adipose tissue. *J Steroid Biochem Mol Biol* 165:369–381.

Abramson FP (1986) Kinetic models of induction: II. decreased turnover of a product or its precursor. *J Pharm Sci* 75:229–232.

Arendse L, Blundell T, and Blackburn, J (2013) Combining in silico protein stability calculations with structure-function relationships to explore the effect of polymorphic variation on cytochrome P450 drug metabolism. *Curr Drug Metab* 14:745-763.

Armas LA, Hollis BW, and Heaney RP (2004) Vitamin D2 is much less effective than vitamin D3 in humans. *J Clin Endocrinol Metab* 89:5387–5391.

Bailie GR and Johnson CA (2002) Comparative review of the pharmacokinetics of vitamin D analogues. In *Seminars in Dialysis*, Vol. 15, pp. 352–357. Wiley Online Library.

Battault S, Whiting SJ, Peltier SL, Sadrin S, Gerber G and Maixent JM (2012) Vitamin D metabolism, functions and needs: from science to health claims. *Eur J Nutr* 52:429–441.

Benaboud S, Urien S, Thervet E, Príe D, Legendre C, Souberbielle JC, Hirt D, Friedlander G, Treluyer JM, and Courbebaisse M (2013) Determination of optimal cholecalciferol treatment in renal transplant recipients using a population pharmacokinetic approach. *Eur J Clin Pharmacol* 69:499–506.

Best CM, Riley DV, Laha TJ, Pflaum H, Zelnick LR, Hsu S, Thummel KE, Foster-Schubert KE, Kuzma JN, Cromer G, Larson I, Hagman DK, Heshelman K, Kratz M, de Boer IH, and Hoofnagle AN (2020) Vitamin D in human serum and adipose tissue after supplementation. *Am J Clin Nutr* 113:83–91.

Bikle D, Halloran B, Gee E, Ryzen E, and Haddad J (1986) Free 25-hydroxyvitamin D levels are normal in subjects with liver disease and reduced total 25-hydroxyvitamin D levels. *J Clin Invest* 78:748.

Bikle DD, Patzek S, and Wang Y (2018) Physiologic and pathophysiologic roles of extra renal CYP27B1: Case report and review. *Bone Reports* 8:255–267.

Cheng J, Levine M, Bell N, Mangelsdorf D, and Russell D (2004) Genetic evidence that the human CYP2R1 enzyme is a key vitamin D 25-hydroxylase. *Proc Natl Acad Sci USA* 101:7711–7715.

Cianferotti L and Marcocci C (2012) Subclinical vitamin D deficiency. *Best Pract Res Cl En* 26:523–537.

Davies B and Morris T (1993) Physiological parameters in laboratory animals and humans. *Pharm Res* 10:1093–1095.

Dawson-Hughes B, Heaney RP, Holick MF, Lips P, Meunier PJ, and Vieth R (2005) Estimates of optimal vitamin D status. *Osteoporos* Int 16:713–716.

Fassio A, Adami G, Rossini M, Giollo A, Caimmi C, Bixio R, Viapiana O, Milleri S, Gatti M, and Gatti D (2020) Pharmacokinetics of oral cholecalciferol in healthy subjects with vitamin D deficiency: a randomized open-label study. *Nutrients* 12:1553.

Ganji V, Zhang X, and Tangpricha V (2012) Serum 25-hydroxyvitamin D concentrations and prevalence estimates of hypovitaminosis D in the US population based on assay-adjusted data. *J Nutr* 142:498–507.

Gao C, Bergagnini-Kolev MC, Liao MZ, Wang Z, Wong T, Calamia JC, Lin YS, Mao Q, and Thummel KE (2017) Simultaneous quantification of 25-hydroxyvitamin D3-3-sulfate and 25-hydroxyvitamin D3-3-glucuronide in human serum and plasma using liquid chromatography–tandem mass spectrometry coupled with DAPTAD-derivatization. *J Chromatogr B* 1060:158–165.

Haq A, Wimalawansa SJ, Pludowski P, and Al Anouti F (2018) Clinical practice guidelines for vitamin D in the United Arab Emirates. *J Steroid Biochem Mol Biol* 175:4–11.

Heaney RP, Horst RL, Cullen DM, and Armas LA (2009) Vitamin D3 distribution and status in the body. *J Am Coll Nutr* 28:252–256.

Heaney RP, Armas LA, Shary JR, Bell NH, Binkley N, and Hollis BW (2008) 25-hydroxylation of vitamin D3: relation to circulating vitamin D3 under various input conditions. *Am J Clin Nutr* 87:1738–1742.

Holick MF (2006) Resurrection of vitamin D deficiency and rickets. *J Clin Invest* 116:2062–2072.

Holick MF (2007) Vitamin D deficiency. *N Engl J Med* 357:266–281.

Holick MF, Biancuzzo RM, Chen TC, Klein EK, Young A, Bibuld D, Reitz R, Salameh W, Ameri A, and Tannenbaum AD (2008) Vitamin D2 is as effective as vitamin D3 in maintaining circulating concentrations of 25- hydroxyvitamin D. *J Clin Endocrinol Metab* 93:677–681.

Holick MF, Binkley NC, Bischoff-Ferrari HA, Gordon CM, Hanley DA, Heaney RP, Murad MH, and Weaver CM (2011) Evaluation, treatment, and prevention of vitamin D deficiency: an Endocrine Society clinical practice guideline. *J Clin Endocrinol Metab* 96:1911–1930.

Hsieh NH, Reisfeld B, Bois FY, and Chiu WA (2018) Applying a global sensitivity analysis workflow to improve the computational efficiencies in physiologically-based pharmacokinetic modeling. *Front Pharmacol* 9:588.

Hsu S, Zelnick LR, Lin YS, Best CM, Kestenbaum B, Thummel KE, Rose LM, Hoofnagle AN, and de Boer IH (2021) Differences in 25-hydroxyvitamin D clearance by eGFR and race: A pharmacokinetic study. *J Am Soc Nephrol* 32:188–198.

Ilahi M, Armas LA, and Heaney RP (2008) Pharmacokinetics of a single, large dose of cholecalciferol. *Am J Clin Nutr* 87:688–691.

Inouye K and Sakaki T (2001) Enzymatic studies on the key enzymes of vitamin D metabolism; 1α-hydroxylase (CYP27B1) and 24-hydroxylase (CYP24). *Biotechnol Annu Rev*. doi: 10.1016/S1387-2656(01) 070375.

Jernigan P and Andress DL (2003) Vitamin D analogs in uremia: integrating medical and nutritional issues. *Adv Ren Replace Ther* 10:241–247.

Jetter A, Egli A, Dawson-Hughes B, Staehelin HB, Stoecklin E, Goessl R, Henschkowski J, and Bischoff-Ferrari HA (2014) Pharmacokinetics of oral vitamin D3 and calcifediol. *Bone* 59:14–19.

Jones G, Prosser DE, and Kaufmann M (2018) The activating enzymes of vitamin D metabolism (25-and 1α-hydroxylases) In *Vitamin D*, pp. 57–79. Elsevier.

Kimura Y, Nakayama M, Kuriyama S, Watanabe S, Kawaguchi Y, and Sakai O (1991) Pharmacokinetics of active vitamins D3, 1 alpha-hydroxyvitamin D3 and 1 alpha, 25-dihydroxyvitamin D3 in patients on chronic hemodialysis. *Clin Nephrol* 35:72–77.

Leow JWH and Chan ECY (2019) Atypical michaelis-menten kinetics in cytochrome P450 enzymes: A focus on substrate inhibition. *Biochem Pharmacol* 169.

Leow JWH, Verma RK, Lim ABH, Fan H, and Chan ECY (2021) Atypical kinetics of cytochrome P450 2J2: Epoxidation of arachidonic acid and reversible inhibition by xenobiotic inhibitors. *Eur J Pharm Sci* 164:105889.

Levine BS and Song M (1996) Pharmacokinetics and efficacy of pulse oral versus intravenous calcitriol in hemodialysis patients. *J Am Soc Nephrol* 7:488–496.

Mawer E, Backhouse J, Holman C, Lumb G and Stanbury S (1972) The distribution and storage of vitamin D and its metabolites in human tissue. *Clin Sci* 43:413–31.

McNally K, Cotton R, and Loizou G (2011) A workflow for global sensitivity analysis of PBPK models. *Front Pharmacol* 2:31.

Meekins ME, Oberhelman SS, Lee BR, Gardner BM, Cha SS, Singh RJ, Pettifor JM, Fischer PR, and Thacher T (2014) Pharmacokinetics of daily versus monthly vitamin D3 supplementation in non-lactating women. *Eur J Clin Nutr* 68:632–634.

Morris MD (1991) Factorial sampling plans for preliminary computational experiments. *Technometrics* 33:161–174.

Munns CF, Shaw N, Kiely M, Specker BL, Thacher TD, Ozono K, Michigami T, Tiosano D, Mughal MZ, Mäkitie O et al. (2016) Global consensus recommendations on prevention and management of nutritional rickets. *Horm Res Paediat* 85:83–106.

Noh K, Yang QJ, Sekhon L, Quach HP, Chow EC, and Pang KS (2020) Noteworthy idiosyncrasies of 1α, 25-dihydroxyvitamin D3 kinetics for extrapolation from mouse to man: Commentary. *Biopharm Drug Dispos* 41:126–148.

Ocampo-Pelland AS, Gastonguay MR, French JF, and Riggs MM (2016) Model-based meta-analysis for development of a population-pharmacokinetic (PPK) model for vitamin D3 and its 25OHD3 metabolite using both in- dividual and arm-level data. *J Pharmacokinet Pharmacodyn* 43:191–206.

Ocampo-Pelland AS, Gastonguay MR, Riggs MM (2017) Model-based meta-analysis for comparing vitamin D2 and D3 parent-metabolite pharmacokinetics. *J Pharmacokinet Pharmacodyn* 44:375–388.

Pérez-López FR, Brincat M, Erel CT, Tremollieres F, Gambacciani M, Lambrinoudaki I, Moen MH, Schenck-Gustafsson K, Vujovic S, Rozenberg S et al. (2012) EMAS position statement: vitamin D and postmenopausal health. *Maturitas* 71:83–88.

Pianosi F, Sarrazin F, and Wagener T (2015) A Matlab toolbox for global sensitivity analysis. *Environ Model Softw* 70:80–85.

Płudowski P, Karczmarewicz E, Bayer M, Carter G, Chlebna-Sokół D, JCzech-Kowalska J, Dębski R, Decsi T, Dobrzańska A, Franek E, et al. (2013) Practical guidelines for the supplementation of vitamin D and the treatment of deficits in Central Europe – recommended vitamin D intakes in the general population and groups at risk of vitamin D deficiency. *Endokrynol. Pol.*, 64:319–327

Quach HP, Yang QJ, Chow EC, Mager DE, Hoi SY, and Pang KS (2015) PKPD modelling to predict altered disposition of 1α,25-dihydroxyvitamin D3 in mice due to dose-dependent regulation of CYP27B1 on synthesis and CYP24A1 on degradation. *Br J Pharmacol* 172:3611–3626.

Ramakrishnan V, Yang QJ, Quach HP, Cao Y, Chow EC, Mager DE, and Pang KS (2016) Physiologically-based pharmacokinetic-pharmacodynamic modeling of 1α, 25-dihydroxyvitamin D3 in mice. *Drug Metab Dispos* 44:189–208.

Rizzoli R, Boonen S, Brandi ML, Bruyère O, Cooper C, Kanis JA, Kaufman JM, Ringe J, Weryha G, and Reginster JY (2013) Vitamin D supplementation in elderly or postmenopausal women: a 2013 update of the 2008 recommendations from the European Society for Clinical and Economic Aspects of Osteoporosis and Osteoarthritis (ESCEO). *Curr Med Res Opin* 29:305–313.

Ross AC (2011) The 2011 report on dietary reference intakes for calcium and vitamin D. *Public Health Nutr*. 14:938–939.

Ross A, Taylor C, Yaktine A, and Del Valle H (2011) Dietary reference intakes for calcium and vitamin D. *Natl Academy Pr*.

Roth DE, Al Mahmud A, Raqib R, Black RE, and Baqui AH (2012) Pharmacokinetics of a single oral dose of vitamin D3 (70,000 IU) in pregnant and non-pregnant women. Nutr J 11:1–15.

Sakaki T, Kagawa N, Yamamoto K, and Inouye K (2005) Metabolism of vitamin D3 by cytochromes P450. *Front Biosci* 10:119–134.

Sawyer ME, Tran HT, and Evans MV (2017) A physiologically based pharmacokinetic model of vitamin D. *J Appl Toxicol* 37:1448–1454.

Schuster I (2011) Cytochromes P450 are essential players in the vitamin D signaling system. *Biochim Biophys Acta, Proteins Proteomics* 1814:186–199.

Sheiner LB and Beal SL (1981) Some suggestions for measuring predictive per-formance. *J Pharmacokinet Biopharm* 9:503–512.

Shinkyo R, Sakaki T, Kamakura M, Ohta M, and Inouye K (2004) Metabolism of vitamin D by human microsomal CYP2R1. *Biochem Biophys Res Commun* 324:451–457.

Society GN (2012) New reference values for vitamin D.

Soulis-Liparota T, Cooper M, Papazoglou D, Clarke B, and Jerums G (1991) Retardation by aminoguanidine of development of albuminuria, mesangial expansion, and tissue fluorescence in streptozocin-induced diabetic rat. *Diabetes* 40:1328–1334.

van Schoor N and Lips P (2018) Worldwide vitamin D status. *Vitamin D* pp. 15–40.

Wang Z, Schuetz EG, Xu Y, and Thummel KE (2013) Interplay between vitamin D and the drug metabolizing enzyme CYP3A4. *J Steroid Biochem Mol Biol* 136:54–58.

Wang Z, Wong T, Hashizume T, Dickmann LZ, Scian M, Koszewski NJ, Goff JP, Horst RL, Chaudhry AS, Schuetz EG, and Thummel KE (2014) Human UGT1A4 and UGT1A3 conjugate 25-hydroxyvitamin D3: Metabolite structure, kinetics, inducibility, and interindividual variability. *Endocrinology* 155:2052–2063.

Wong T, Wang Z, Chapron BD, Suzuki M, Claw KG, Gao C, Foti RS, Prasad B, Chapron A, Calamia J, Chaudhry A, Schuetz EG, Horst RL, Mao Q, de Boer IH, Thornton TA, and Thummel KE (2018) Polymorphic human sulfotransferase 2A1 mediates the formation of 25-hydroxyvitamin D3-3- O-Sulfate, a major circulating vitamin D metabolite in humans. *Drug Metab Dispos* 46:367-379.

DMD Fast Forward. Published on July 2, 2022 as DOI: 10.1124/dmd.121.000609
This article has not been copyedited and formatted. The final version may differ from this version.

13 Footnotes

a.) This research was supported by the National Institutes of Health [R01 GM107122] (MSJ, TDN). No author has an actual or perceived conflict of interest with the contents of this article.

b.) Sawyer CW, Tuey SM, West III RA, Nolin TD, Joy MS. A Triphasic Physiologically Based Pharmacokinetic Model of Vitamin D3 and Metabolites in Vitamin D Insufficient Patients. Presented at *BAMM! Biology and Medicine through Mathematics*, Richmond, VA, May 19, 2022.

c.) Colton W. Sawyer; 2500 N. River Rd, Manchester, NH 03106, USA. **c.sawyer1@snhu.edu**

d.)

DMD Fast Forward. Published on July 2, 2022 as DOI: 10.1124/dmd.121.000609
This article has not been copyedited and formatted. The final version may differ from this version.

14 Figure Legends

Figure 1: General physiologically based pharmacokinetic model diagram for $VitD_3$ and metabolites. Symbols are defined as the following: Q is the plasma flow rate, C_{ap} is the arterial concentration of the compound; $C_{vp:T} = A_T/(V_T * P_T)$ is the apparent concentration of the compound in tissue T defined as the amount of compound divided by the volume of the tissue times the tissue:plasma partition coefficient; k_a is the absorption rate from the gut.

Figure 2: Network diagram for the $VitD_3$ metabolic cascade model. The network contains compounds with measured concentrations and black arrows define conversion steps with kinetic equations as defined in Table 2. Note that concentrations of $1,24,25(OH)_3D_3$ were not measured in this study.

Figure 3: Predicted PBPK plasma concentrations for $VitD_3$ metabolites ($25D_3$, $24,25D_3$, and $1,25D_3$). Box plots indicate the middle 50% of the data with the median data indicated by a line, and the shading indicates the 95% confidence interval of the model predictions. Insets indicate enhanced view of data for predicted PBPK plasma concentrations for $VitD_3$ metabolites ($25D_3$, $24,25D_3$, and $1,25D_3$), clipping out the supplementation period from days 20 through 92 of the experiment, where the wavy line in the center indicates the clipped portion of the model during the supplementation period where no data were observed.

(a) $25D_3$ serum levels (nmol L^{-1})

(b) $24,25D_3$ serum levels (nmol L^{-1})

(c) $1,25D_3$ serum levels (nmol L^{-1})

Figure 4: Observed plasma concentrations versus predicted PBPK plasma concentrations in vitamin and three metabolites. Red x-marks indicate observations from the deficient period, blue circles indicate observations from the replete period, the dotted line represents the identity line and the green lines represent the 2-fold interval.

Figure 5: Simulation of daily 1000 I.U. dosing regimen. Solid line indicates model predictions, data taken from [Holick et al., 2008] are mean ± SEM.

DMD Fast Forward. Published on July 2, 2022 as DOI: 10.1124/dmd.121.000609
This article has not been copyedited and formatted. The final version may differ from this version.

15 Tables

Table 1: Baseline characteristics of study participants (n = 11)

Study Site	University of Pittsburgh	9 (82%)
	University of Colorado	2 (18%)
Gender	Female	6 (55%)
	Male	5 (45%)
Race	White	6 (55%)
	Black	5 (45%)
Ethnicity	Non-Hispanic	11 (100%)
Age (years)		57 (11.5)
Weight (kg)		89.2 (42.6)
BMI (kg/m^2)		30.5 (13.2)
eGFR (ml/min/1.73 m^2)		92 (10.5)
Serum Albumin (g/dl)		4.3 (0.2)
Serum VDBP (μg/ml)		294 (88.7)

Data are presented as median (IQR) or number (%).

Abbreviations: eGFR – estimated glomerular filtration rate; VDBP – vitamin D binding protein

DMD Fast Forward. Published on July 2, 2022 as DOI: 10.1124/dmd.121.000609
This article has not been copyedited and formatted. The final version may differ from this version.

Table 2: Kinetic parameters for the PBPK model. Optimized parameters are given with bootstrapped 95% confidence intervals and all other parameters are held to available literature values or estimates as notated. Note the 95% CIs are not necessarily symmetric about the optimized parameter due to the method of sampling. See the *Model simulations and parameter estimations* section for details.

Parameter	Description	Value	Units	Reference
K_m	Michaelis-Menten constant for CYP2R1	5.91[a] (5.09, 5.95)	nmol L^{-1}	Optimized
D_{base}	Endogenous baseline concentration of $VitD_3$	2.05[a] (2.00, 2.06)	nmol·L^{-1}	Optimized
k_a	Absorption constant	0.32	h^{-1}	[Ocampo-Pelland et al., 2016]
R_{27B1}^{25}	Synthesis of $25D_3$ to $1,25D_3$ by CYP27B1	17.7[b] (15.85, 18.97)	L·hr^{-1}	Optimized
f_{ub}^{25}	Percent free unbound $25D_3$	0.03	--	[Bikle et al., 1986]
Synthesis of $24,25D_3$ from $25D_3$ by CYP24A1 in tissue				
$R_{24A1,L}^{25}$	Liver	10.2[b] (8.45, 10.8)	L·hr^{-1}	Optimized
$R_{24A1,K}^{25}$	Kidney	2.43[b] (2.06, 2.68)	L·hr^{-1}	Optimized
$R_{24A1,Br}^{25}$	Brain	13.3[b] (12.2, 13.9)	L·hr^{-1}	Optimized
$R_{24A1,I}^{25}$	Intestine	15.4[b] (13.2, 16.8)	L·hr^{-1}	Optimized
Clearance of unbound (free) $1,25D_3$ by CYP24A1 in tissue T, $CL_{free,int,T}^{125}$				
$CL_{free,int,L}^{125}$	Liver	0.0057	mL·hr^{-1}·g^{-1}	[Noh et al., 2020]

DMD Fast Forward. Published on July 2, 2022 as DOI: 10.1124/dmd.121.000609
This article has not been copyedited and formatted. The final version may differ from this version.

$CL^{125}_{free,int,K}$	Kidney	0.066[a] (0.065, 0.082)	mL·hr^{-1}·g^{-1}	Optimized
$CL^{125}_{free,int,Br}$	Brain	0.0083	mL·hr^{-1}·g^{-1}	[Noh et al., 2020]
$CL^{125}_{free,int,I}$	Intestine	0.0028	mL·hr^{-1}·g^{-1}	[Noh et al., 2020]
$CL^{2425}_{free,int,K}$	Clearance of unbound (free) 24,25D	990[b] (946, 1068)	pmol·hr^{-1}	Optimized
I_{max}	Maximal inhibitory effect of CYP27B1	1	fold change	[Noh et al., 2020]
IC_{50}	Total 1,25D$_3$ concentration when reaching 50% *Imax*	672[a] (680,1068)	pmol L^{-1}	Optimized
Maximal stimulatory effect of CYP24A1 in tissue T, $E_{max,T}$				
$E_{max,L}$	Liver	122[a] (88.7, 131.6)	fold change	Optimized
$E_{max,K}$	Kidney	25[a] (23.9, 28.0)	fold change	Optimized
$E_{max,Br}$	Brain	22[a] (21.5, 23.0)	fold change	Optimized
$E_{max,I}$	Intestine	675	fold change	[Noh et al., 2020]
Total tissue 1,25D$_3$ concentration when reaching 50% E_{max}, $EC_{50,T}$				
$EC_{50,L}$	Liver	2600	pmol L^{-1}	[Noh et al., 2020]
$EC_{50,K}$	Kidney	143	pmol L^{-1}	[Noh et al., 2020]
$EC_{50,Br}$	Brain	97[a] (74.5, 97.5)	pmol L^{-1}	Optimized
$EC_{50,I}$	Intestine	2640	pmol L^{-1}	[Noh et al., 2020]
Hill coefficient of CYP24A1 in tissue T, $\gamma_{1,T}$				

DMD Fast Forward. Published on July 2, 2022 as DOI: 10.1124/dmd.121.000609
This article has not been copyedited and formatted. The final version may differ from this version.

$\gamma_{1,L}$	Liver	3.05[a] (2.99, 3.47)	--	Optimized
$\gamma_{1,K}$	Kidney	3.59	--	[Noh et al., 2020]
$\gamma_{1,Br}$	Brain	1.12[c] (0.90, 1.15)	--	Optimized
$\gamma_{1,I}$	Intestine	4.16	--	[Noh et al., 2020]
γ_2	Hill coefficient of CYP27B1	2.7	--	[Noh et al., 2020]
$k_{out,27}$	Turnover rate constant of CYP27B1	0.245	h^{-1}	[Noh et al., 2020]
Turnover rate constant of CYP24A1 in tissue T, $k_{out}^{24,T}$				
$k_{out,24,L}$	Liver	0.47	h^{-1}	[Noh et al., 2020]
$k_{out,24,K}$	Kidney	0.28	h^{-1}	[Noh et al., 2020]
$k_{out,24,Br}$	Brain	0.86	h^{-1}	[Noh et al., 2020]
$k_{out,24,I}$	Intestine	0.047	h^{-1}	[Noh et al., 2020]
Atypical Kinetic Parameters for V_{max}				
V'	Maximum value of V_{max} for CYP2R1	5.76[b] (5.73, 5.76)	L hr^{-1}	Optimized
D_{50}	Concentration at which 50% of V' occurs	8.35[b] (8.34, 8.35)	nmol L^{-1}	Optimized
h_V	Hill constant for variable V_{max}	2.27[b] (2.26, 2.27)	--	Optimized
Dynamic Adipose partition coefficient parameters				
$Adi_{D,max}$	Maximum adipose PC for $VitD_3$	9.9[b] (9.78, 10.4)	--	Optimized
$Adi_{25,max}$	Maximum adipose PC for $25D_3$	1.64[b] (0.90, 1.73)	--	Optimized

DMD Fast Forward. Published on July 2, 2022 as DOI: 10.1124/dmd.121.000609
This article has not been copyedited and formatted. The final version may differ from this version.

$Adi_{D,50}$	Concentration at which 50% of $Adi_{D,max}$ occurs	8.96[b] (4.93, 11.98)	nmol L^{-1}	Optimized
$Adi_{25D,50}$	Concentration at which 50% of $Adi_{25D,max}$ occurs	117[b] (61.8, 121)	nmol L^{-1}	Optimized
h_D	Hill constant for $AdiPC_D$	2.12[b] (2.10, 2.30)	--	Optimized
h_{25}	Hill constant for $AdiPC_{25}$	0.96[b] (0.86, 1.01)	--	Optimized

Abbreviations: D_3, $VitD_3$; $25D_3$, $25(OH)D_3$; $1,25D_3$, $1,25(OH)_2D_3$; $24,25D_3$, $24,25(OH)_2D_3$

[a]Confidence interval does not contain literature values

[b]No literature values available for comparison

[c]Confidence interval contains literature value

DMD Fast Forward. Published on July 2, 2022 as DOI: 10.1124/dmd.121.000609
This article has not been copyedited and formatted. The final version may differ from this version.

16 Figures

Attached separately

DMD Fast Forward. Published on July 2, 2022 as DOI: 10.1124/dmd.121.000609
This article has not been copyedited and formatted. The final version may differ from this version.

18 Appendix

A.1 PBPK Model Equations

The parameters in the PBPK model equations refer to tissue (T), arterial blood flow (Q), compound amount (A), concentration (C), volume (V), and tissue:plasma partition coefficients ($P_{T:p}$). The concentration in each tissue is given by Equation (A1), where the tissue:plasma partition coefficients are given in Supp. Table S2.

$$C_T = A_T/(V_T \cdot P_{T:p}) \tag{A1}$$

For compartments that have the same equation form across all compounds, general mass balance differential equations are given in Equations (A2) and (A3) based on Figure 1 in the main text. Definitions and values for parameter values for Equations (A2) through (A14) are given in Table 2 and Supp. Tables S1 and S2.

Non-eliminating tissue in the set Z (adipose, heart, rapidly perfused, slowly perfused)

$$V_Z \cdot \mathrm{d}C_Z/\mathrm{d}t = BP \cdot Q_Z \cdot (C_p - C_{p:Z}) \tag{A2}$$

Plasma:

$$V_p \cdot \mathrm{d}C_p/\mathrm{d}t = \Sigma_T [BP \cdot Q_T \cdot C_{p:T}] - \mathrm{BP} \cdot Q_{CO} \cdot C_p \tag{A3}$$

Equations (A4) through (A7) describe the mass balance equations for the remaining four compartments (brain [Br], intestines [I], kidney [K], liver [L]) for $VitD_3$ and each metabolite, where additional components are described in Equations (A8) through (A14).

$VitD_3$ equations:

$$V_{Br} \cdot \mathrm{d}C_{Br}/\mathrm{d}t = BP \cdot Q_{Br} \cdot (C_p - C_{p:Br}) \tag{A4a}$$

$$V_I \cdot \mathrm{d}C_I/\mathrm{d}t = BP \cdot Q_I \cdot (C_p - C_{p:I}) + k_a \cdot A_{gut} \tag{A4b}$$

$$V_K \cdot \mathrm{d}C_K/\mathrm{d}t = BP \cdot Q_K \cdot (C_p - C_{p:K}) \tag{A4c}$$

$$V_L \cdot \mathrm{d}C_L/\mathrm{d}t = BP \cdot Q_L \cdot (C_p - C_{p:L}) + ENDOG - R25D \tag{A4d}$$

$25D_3$ equations:

$$V_{Br} \cdot \mathrm{d}C_{Br}/\mathrm{d}t = BP \cdot Q_{Br} \cdot (C_p - C_{p:Br}) - R2425D_{Br} \tag{A5a}$$

$$V_I \cdot \mathrm{d}C_I/\mathrm{d}t = BP \cdot Q_I \cdot (C_p - C_{p:I}) - R2425D_I \tag{A5b}$$

$$V_K \cdot \mathrm{d}C_K/\mathrm{d}t = BP \cdot Q_K \cdot (C_p - C_{p:K}) - R125D - R2425D_K \tag{A5c}$$

DMD Fast Forward. Published on July 2, 2022 as DOI: 10.1124/dmd.121.000609
This article has not been copyedited and formatted. The final version may differ from this version.

$$V_L \cdot \mathrm{d}C_L/\mathrm{d}t = BP \cdot Q_L \cdot (C_p - C_{p:L}) + R25D_3 - R2425D_L \quad \text{(A5d)}$$

24,25D_3 equations:

$$V_{Br} \cdot \mathrm{d}C_{Br}/\mathrm{d}t = BP \cdot Q_{Br} \cdot (C_p - C_{p:Br}) + R2425D_{Br} \quad \text{(A6a)}$$

$$V_I \cdot \mathrm{d}C_I/\mathrm{d}t = BP \cdot Q_I \cdot (C_p - C_{p:I}) + R2425D_I \quad \text{(A6b)}$$

$$V_K \cdot \mathrm{d}C_K/\mathrm{d}t = BP \cdot Q_K \cdot (C_p - C_{p:K}) + R2425D_K - CL2425D_{Br} \quad \text{(A6c)}$$

$$V_L \cdot \mathrm{d}C_L/\mathrm{d}t = BP \cdot Q_L \cdot (C_p - C_{p:L}) + R2425D_L \quad \text{(A6d)}$$

1,25D_3 equations:

$$V_{Br} \cdot \mathrm{d}C_{Br}/\mathrm{d}t = BP \cdot Q_{Br} \cdot (C_p - C_{p:Br}) - CL125D_{Br} \quad \text{(A7a)}$$

$$V_I \cdot \mathrm{d}C_I/\mathrm{d}t = BP \cdot Q_I \cdot (C_p - C_{p:I}) - CL125D_I \quad \text{(A7b)}$$

$$V_K \cdot \mathrm{d}C_K/\mathrm{d}t = BP \cdot Q_K \cdot (C_p - C_{p:K}) + R125D - CL125D_K \quad \text{(A7c)}$$

$$V_L \cdot \mathrm{d}C_L/\mathrm{d}t = BP \cdot Q_L \cdot (C_p - C_{p:L}) - CL125D_L \quad \text{(A7d)}$$

Additional differential equations for the PBPK model are given in Equations (A8) to (A14), where concentrations in tissue *T* are indicated by $[M_T]$ where *M* is VitD_3 or a metabolite:

Absorption of VitD_3:

$$\mathrm{d}A_{gut}/\mathrm{d}t = - k_a \cdot A_{gut} \quad \text{(A8)}$$

Endogenous production of VitD_3:

$$ENDOG = \frac{V_{max} * [D_{base}]}{K_m + [D_{base}]} * [D_{base}] \quad \text{(A9)}$$

Conversion of VitD_3 to 25D_3 in the liver (*L*):

$$R25D = \frac{V_{max} * [D_L]}{K_m + [D_L]} * [D_L] \quad \text{(A10)}$$

Conversion of 25D_3 to 1,25D_3 in kidney by CYP27B1:

$$R125\mathrm{D} = R_{27B1}^{25} \cdot [25D_K] \cdot f_{ub}^{25} \cdot CYP27B1_{FC} \quad \text{(A11)}$$

Conversion of 25D_3 to 24,25D_3 in tissue *T* by CYP24A1:

$$R2425D_{\mathrm{T}} = R_{24A1,T}^{25} \cdot [25D_T] \cdot f_{ub}^{25} \cdot CYP24A1_{FC,T} \quad \text{(A12)}$$

Clearance of 1,25D_3 in tissue *T* by CYP24A1:

$$CL125D_T = CL_{free,int,T}^{125} \cdot [1,25D_T] \cdot CYP24A1_{FC,T} \quad \text{(A13)}$$

DMD Fast Forward. Published on July 2, 2022 as DOI: 10.1124/dmd.121.000609
This article has not been copyedited and formatted. The final version may differ from this version.

Clearance of 24,25D_3 in the kidney:

$$CL2425\mathrm{D} = CL^{2425}_{free,int,K} \cdot [24{,}25D_K] \quad \text{(A14)}$$

The initial conditions for the model were generated by taking the mean of the data points to generate an initial estimate for the median plasma concentration.

DMD Fast Forward. Published on July 2, 2022 as DOI: 10.1124/dmd.121.000609
This article has not been copyedited and formatted. The final version may differ from this version.

Figure 1

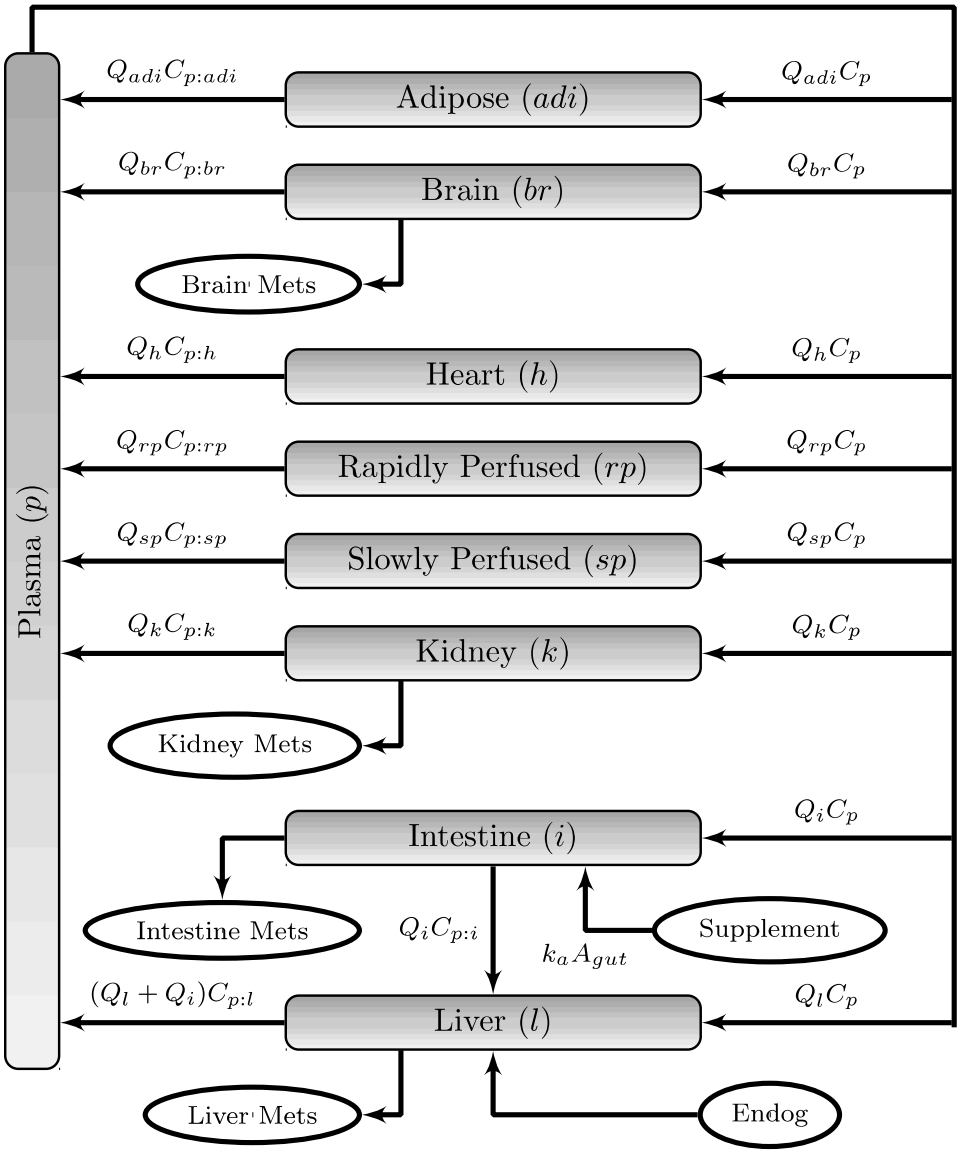

DMD Fast Forward. Published on July 2, 2022 as DOI: 10.1124/dmd.121.000609
This article has not been copyedited and formatted. The final version may differ from this version.

Figure 2

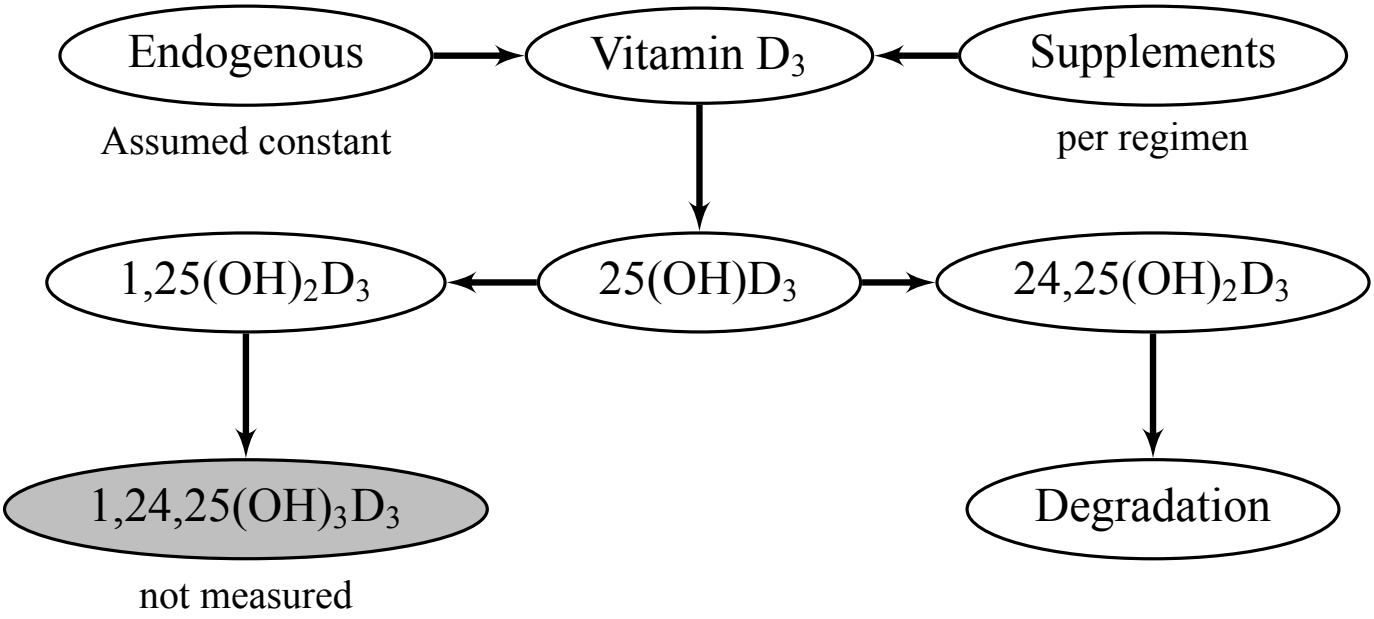

DMD Fast Forward. Published on July 2, 2022 as DOI: 10.1124/dmd.121.000609
This article has not been copyedited and formatted. The final version may differ from this version.

Figure 3

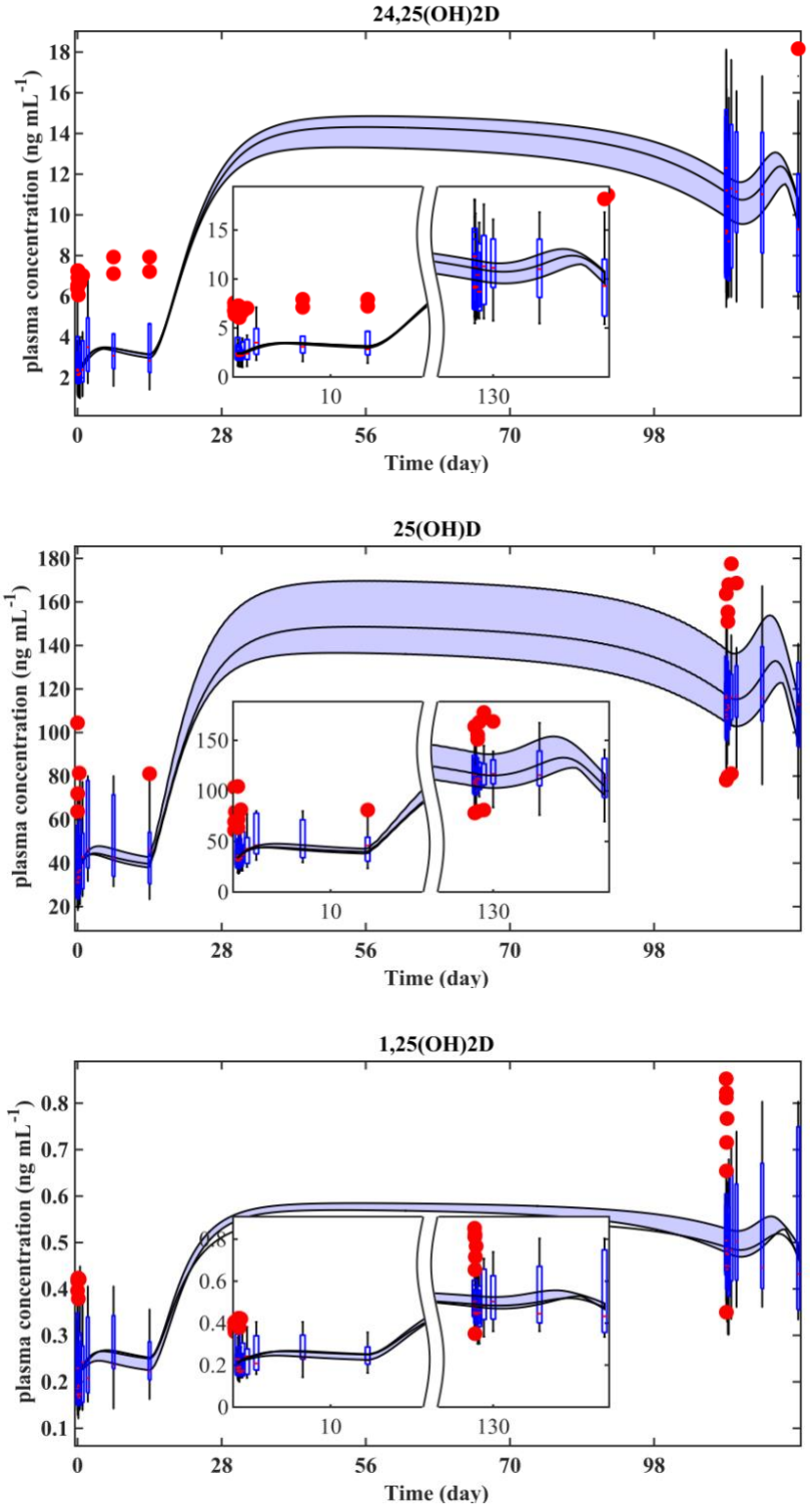

DMD Fast Forward. Published on July 2, 2022 as DOI: 10.1124/dmd.121.000609
This article has not been copyedited and formatted. The final version may differ from this version.

Figure 4

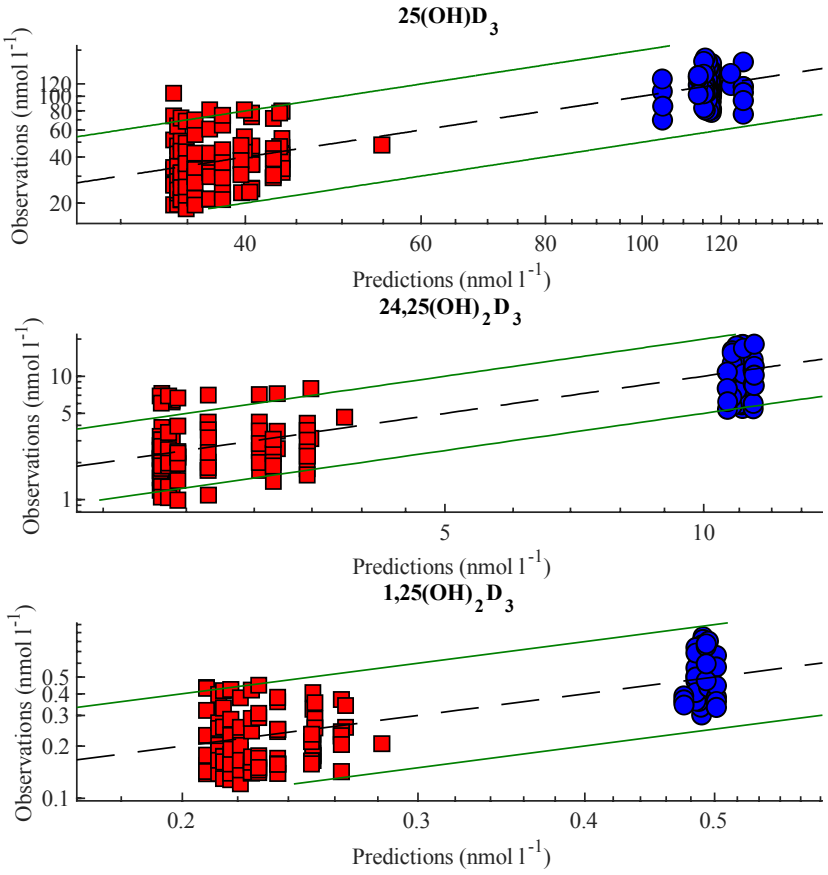

DMD Fast Forward. Published on July 2, 2022 as DOI: 10.1124/dmd.121.000609
This article has not been copyedited and formatted. The final version may differ from this version.

Figure 5